

Radar Detection of Plasma-Covered Reentry Object Based on Crossed Two-Component LFM Signal

Xuyang Chen¹, Fangfang Shen¹, Yanming Liu¹, Xiaoping Li¹, and Wei Ai²

¹ School of Aerospace Science and Technology
Xidian University, Xi'an, Shaanxi 710071, China
xychen@mail.xidian.edu.cn, ffshen@mail.xidian.edu.cn, ymliu@xidian.edu.cn, xpli@xidian.edu.cn

² Science and Technology on Space Physics Laboratory
China Academy of Launch Vehicle Technology, Beijing 100076, China
27821126@qq.com

Abstract — A precise and efficient radar detection method based on crossed two-component LFM signal is proposed to deal with the detection problem of plasma-covered object. The method contains two segments: 1) design of transmitted signal, and 2) detection of object information (position and velocity) from the ambiguity function of the echo signal. For the first segment, the transmitted signal is designed to be a 2-component LFM signal with each component crossing with the other one in the time-frequency domain. The crossing design of the two components eliminates the disturbance term in solving the ambiguity function, guaranteeing the stability of detection. In the second segment, a mixed detection technique is proposed, which contains prior-information-based component classification and optimal parameters solution, maintaining both the accuracy and efficiency in detection. By the proposed method, both the efficiency in computation and accuracy in detection are achieved. The simulation results illustrate the validity of the method.

Index Terms— Crossed two-component LFM signal, plasma sheath, radar detection, reentry object.

I. INTRODUCTION

The radar detection of plasma-covered reentry object arouses great attention in recent decade years with the development of applications like spacecraft recycle and radar surveillance. The emphasis in this research field lies in the study of the effect and its solution of plasma sheath on radar echo. Several researchers [1-6] carried out their work in this field and reveal some effect rules, including magnitude attenuation, dispersion in frequency, which may cause the deviation or failure in detection of object. However, these works mainly focused on the effect study of plasma sheath but few gave the way to overcome the effect. Certainly, there are some methods that can be used to deal with the plasma

sheath effect to some extent, like appending magnetic field [7,8] and changing the antenna assembly of object [9]. Unfortunately, these methods are proposed to deal with the communication breakout problem but not suitable for the radar detection problem.

In our previous work [10], we proposed an idea of utilizing multi-component linear-frequency-modulation (LFM) signal to detect the radar echo of plasma-covered objects. The motivation of the idea is the consideration of the influence rule of plasma sheath on ambiguity function of the echo signal reflected by a plasma-covered object. The rule can be summarized as following: the plasma sheath can exert significant influence on the 2-D time-frequency position of the maximal point of ambiguity function, but its effect on the 2-D structure of energy distribution is trivial. Under this consideration, we found that, by using the multi-component LFM signal [11-16] as the transmitted signal, one can produce an ambiguity function with stable and detectable structure, which is a more suitable way to detect the plasma-covered object. However, the work in Ref. [10] is preliminary and leaves a key problem about how to detect the object from the echo for the case of multi-component LFM signal as transmitted signal.

There are several methods which can be used to detect the multi-component LFM signal, including fractional Fourier transform (FRFT) [12-14], Wigner-Hough transform (WHT) [15], Radon transform [16], etc. These methods are effective in solving the parameters of each component of the composite LFM signal. However, they have a common weakness, that is: the estimation precision of the parameters of components strongly relies on the setup of the increment of rotation angle and displacement quantity. A higher parameter precision means a smaller increment which implies a more complexity in calculation, restricting its real-time detection application. But the radar detection of reentry object, considered in this paper, requires both the

precision and real-time capability. Thus, these common methods mentioned above are not suitable for solving the detection problem in this paper.

Maintaining both the detection precision (or accuracy) and the real-time capability in the detection of multi-component LFM signal is an intractable problem. We tackle this problem only for the 2-component LFM signal in this paper. This is because the 2-component LFM signal is enough to acquire the stability and detectability in structure of the ambiguity function for the detection of plasma-covered object.

In this paper, we propose a precise and efficient radar detection method of plasma-covered object based on crossed 2-component LFM signal. The detection method contains two parts: 1) the design of transmitted signal, and 2) the detection of object information (position and velocity) from the ambiguity function of the echo signal reflected by a plasma-covered object. For the first part, the transmitted signal is designed to be a 2-component LFM signal with each component of the signal crossing with the other one in the time-frequency domain of ambiguity function. The crossing design of the two components eliminates the disturbance term in solving the ambiguity function, guaranteeing the stability of detection. For the second part, to maintain both the precision and efficiency in detection, we propose a mixed detection technique containing the prior-information-based component classification and the optimal parameters solution. By the proposed method, both the efficiency and accuracy in detection are achieved. The simulation results illustrate the validity of the method.

II. BACKGROUND OF RADAR DETECTION OF A PLASMA-COVERED OBJECT

Let a transmitted radar signal be $s(t)$. When the signal $s(t)$ meets with a plasma-covered reentry object, an echo signal $r(t)$ is generated. The relation of $r(t)$ and $s(t)$ can be expressed as follows [6]:

$$r(t) = [s(t) \otimes l(t) \otimes p(t)] \cdot \exp(j2\pi f_d t), \quad (1)$$

where t is the time variable within one pulse repetition interval (PRI) of a radar system, the sign ' \otimes ' represents convolution, $l(t)$ denotes the effect of space distance, $p(t)$ is the effect of the plasma surrounding the object to be detected, and f_d is the Doppler frequency caused by the velocity of the object.

Generally, the plasma effect on a radar echo is described by the reflection coefficient of plasma $\hat{p}(f)$ in frequency domain, expressed by

$$\hat{p}(f) = |\hat{p}(f)| \exp(j\varphi_p(f)), \quad (2)$$

where $|\hat{p}(f)|$ is the magnitude of $\hat{p}(f)$ and $\varphi_p(f)$ is the phase of $\hat{p}(f)$. Note, the $p(t)$ in (1) is a time-domain expression and it is the Inverse Fourier Transform of

$\hat{p}(f)$.

The plasma affects a radar echo both on the magnitude and on the phase. Figure 1 shows an example of the plasma effect based on the measurement data of 'RAM-C' experiment [17]. The label 'Diff. Phase' in Fig. 1 means the differential phase which reflects the change of phase. The 'Max Ne' denotes the maximal electron density of plasma, which is an important plasma parameter and is usually varying in a reentry flight of an object. Clearly, the plasma causes magnitude attenuation as well as phase jump in frequency domain, as shown in Fig. 1.

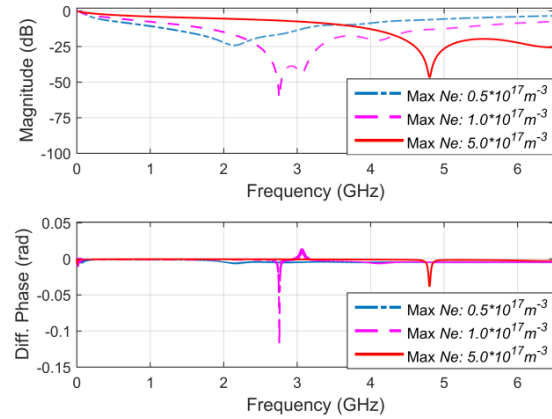


Fig. 1. An example of the plasma effect on echo signal both on magnitude (top figure) and on phase (bottom figure) in frequency domain.

To further reveal the plasma effect on radar detection, we then give the introduction of radar signal and that of ambiguity function analysis as follows. The LFM signal (with one component), as a common transmitted radar signal, is expressed as the form:

$$s(t) = A \exp(j(2\pi f_0 t + \frac{\pi}{T} B t^2)), \quad (3)$$

where the symbols A , f_0 , T , and B are the amplitude, center frequency, pulse width, and bandwidth of the transmitted signal, respectively.

The ambiguity function analysis of echo signal is a popular and useful method in radar detection, by which the object information about the position (reflected from the time delay) and the velocity (reflected from the Doppler frequency) of the object can both be determined. In addition, the resolution of the echo signal in the 2-D time-frequency domain can also be revealed from ambiguity function. Let the ambiguity function of echo $r(t)$ be $\chi(\tau, f)$, expressed by:

$$\chi(\tau, f) = \int_{-\infty}^{+\infty} s(t) r^\dagger(t + \tau) \exp(j2\pi f t) dt, \quad (4)$$

where the superscript ' \dagger ' denotes complex conjugation, and τ and f are the time delay and frequency shift,

respectively. By detecting the peak of the magnitude of $\chi(\tau, f)$, one can estimate the true time delay and the true Doppler frequency of an object to be detected. Certainly, the environmental interference or noise (such as the plasma effect considered here) may influence the estimation error.

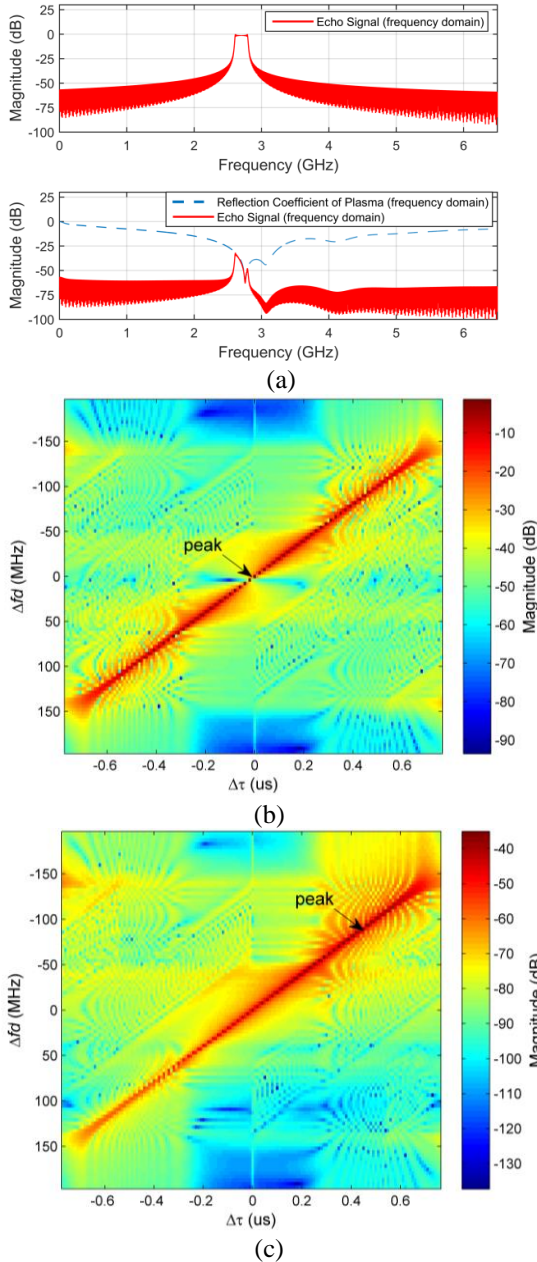


Fig. 2. Comparison of echo signal without plasma effect and that with plasma effect in magnitude. (a) Magnitude of echo signal without (top) and with (bottom) plasma effect in frequency domain. (b) Magnitude of echo signal without plasma effect in time-frequency domain. (c) Magnitude of echo signal with plasma effect in time-frequency domain.

Note: the echo signal $r(t)$ as well as the transmitted signal $s(t)$ in (4) are usually of intermediate frequency form in realistic radar system, which implies a down-conversion operation with a frequency f_{down} . Whatever f_{down} is, it only results in an additional oscillation with fixed frequency on the whole ambiguity function $\chi(\tau, f)$ but not affects the energy distribution of $\chi(\tau, f)$. With this in mind, we omit the down-conversion frequency f_{down} in (4).

Figure 2 shows a comparison of echo signal without plasma effect and that with plasma effect in the frequency domain and in the time-frequency domain solved by ambiguity function. The plasma effect in the figure is selected to be a severe case to obtain an obvious comparison (the same with that described by the purple dashed line in Fig. 1). The transmitted signal is selected to be a LFM signal with parameters: $f_0 = 2.7\text{GHz}$, $B = 200\text{MHz}$, and $T = 1\mu\text{s}$. The horizontal coordinate and vertical coordinate of the ambiguity function (sub-figure (b), (c)) are the time axis (denoted by $\Delta\tau$) and frequency axis (denoted by Δf_d), respectively. Note: the true time delay and true Doppler frequency in the ambiguity function are both set to be zero here to make the comparison clear.

It can be found from Fig. 2 (a), compared with the echo signal in the top sub-figure, that in the bottom sub-figure has an obvious magnitude distortion and attenuation in frequency band due to the plasma effect. From the comparison of Fig. 2 (b) and Fig. 2 (c), it is clear that the peak of the ambiguity function is shifted largely in the time-frequency domain, also the magnitude of the major energy distribution is attenuated. The effect of plasma will result in distinct deviation in detection of the object in position and velocity.

III. RADAR DETECTION OF PLASMA-COVERED OBJECT BASED ON CROSSED TWO-COMPONENT LFM SIGNAL

A. Design of transmitted signal

As shown in the Introduction section, the proposed radar detection method contains two parts, shorted by signal design and object detection here. The object detection is obviously the key of the proposed detection method, by which the object information of an echo hidden in its time-frequency structure is extracted. Before the presentation of the object detection, the signal design has to be introduced firstly.

As indicated in our previous work [10], the peak point of ambiguity function of echo signal in magnitude is sensitive to the plasma effect, but its 2-D structure of energy distribution is insensitive to the plasma effect. Thus, if one can design a transmitted signal with a robust and detectable structure, the plasma effect will be reduced significantly. To meet this requirement, we

designed a 2-component LFM signal as follows:

$$s(t) = A \sum_{i=1}^2 \exp(j(2\pi f_0 t + (-1)^i \frac{\pi}{T} B t^2)), t \in [-\frac{T}{2}, \frac{T}{2}], (5)$$

where A , B , T , and f_0 are the common amplitude, bandwidth, pulse width and center frequency of the two components. Note: the two components in (5) are designed to cross with each other in time-frequency domain, which suppresses the generation of disturbance term in time-frequency domain.

Figure 3 shows an example of ambiguity function for such an echo signal (without plasma effect). The setup of parameters is same with that in Fig. 2 except for the signal type changing to two-component LFM signal. As shown in Fig. 3, the two components of LFM signal cross with each other, with the crossing point at the center of each component, complying with (5).

The horizontal coordinate and vertical coordinate of the crossing point in Fig. 3 represent the true time delay (reflecting the true position of object) and the true Doppler frequency (reflecting the true velocity of object), respectively. Therefore, the object information (including the true position and velocity of the object) can be extracted by detection of the crossing point of the two components. Actually, detecting the crossing point of the two components is equivalent to detecting the structure of the 2-D energy distribution of the LFM signal in ambiguity function. This is because the crossing point, as a main quantitative expression of the crossing characteristic of the 2-D energy structure, possesses a stable and robust position (2-D coordinate), reflecting the stability of the structure. Clearly, the shift of the energy peak of any one component along its main energy region (a 'line') cannot affect the position of the crossing point, reflecting its stability.

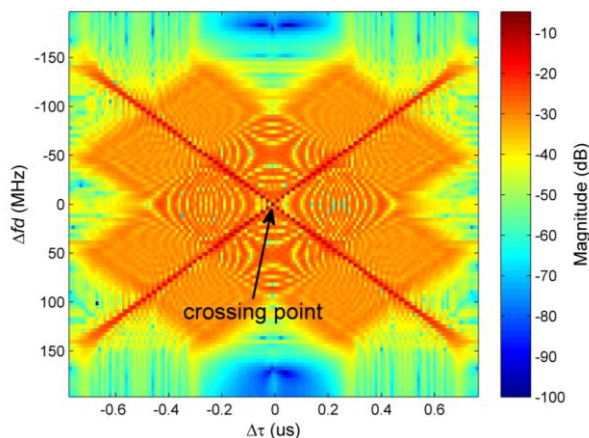


Fig. 3. The magnitude of ambiguity function of echo signal for the case of a two-component LFM signal as the transmitted signal (without plasma effect).

B. Detection method based on crossed two-component LFM signal

As stated in Sec. III-A, the crossing point of the two components of the LFM signal contains the information of true time delay and that of true Doppler frequency. However, the direct detection of the crossing point with high precision is a difficult problem. We tackle this problem from the following thinking: the parameters of the two components can be calculated at first, with which an equation set is generated; by solving the equation set, one can work out the crossing point. The key problem in the thinking is how to obtain an efficient and accurate estimation (or calculation) of the parameters of the two components.

To deal with the problem, we propose a mixed detection method containing prior-information-based component classification and optimal parameters solution. Different from the scenarios in Ref. [12-16], in the detection application of this paper, we have an important prior information about the echo signal reflected from a plasma-covered object. That is: the echo signal is initially produced from a transmitted signal whose parameters (center frequency, bandwidth, and pulse width) is known in advance. There are differences between the echo signal and the transmitted signal due to plasma effect. But, the differences are minor from the view of the whole 2-D time-frequency ranges where the main echo energy locates (see Fig. 3).

In detail, the available information which can be used as prior information is listed as two parts as below.

- From the aspect of actual application, the Doppler frequency shift in an echo signal relative to the bandwidth of its corresponding transmitted signal is significantly small, making it possible to partition the 2-D time-frequency figure of the echo signal along the Doppler frequency axis.
- The bandwidth B and pulse width T of the transmitted signal determine the slope of the two 'energy lines' of the main energy regions of ambiguity function to be $\pm \frac{B}{T}$.

By utilizing the 'part a' prior information shown above, we will classify all the available peak points in the two 'energy lines' of echo signal in the 2-D time-frequency domain. A schematic diagram about the procedure has been drawn in Fig. 4. As shown in the figure, we first partition the 2-D time-frequency figure along the time axis (horizontal axis) to obtain two valid regions and one fuzzy region. Then we pick all the valid peak points from the leftmost column to the rightmost column of the data in the valid region of $|\chi(\tau, f)|$. Only those peak points lying in the two 'energy lines' (marked by 'line1' and 'line2') are thought to be valid and can be picked. Note that the 'lines' composed of the picked

points are broken off by the fuzzy region, forming a fracture region along the vertical axis. Finally, we classify all the picked points into their corresponding 'energy lines' ('line1' or 'line2') according to separation effect caused by the fuzzy region and the fracture region.

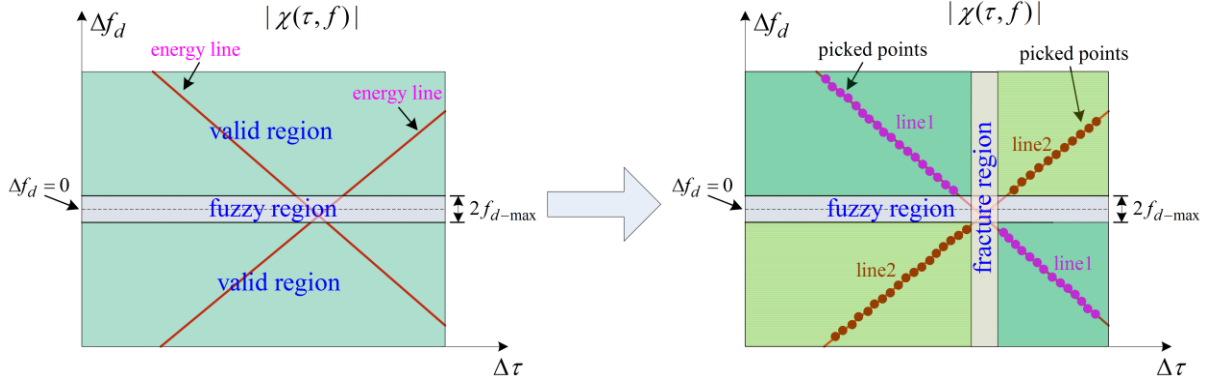


Fig. 4. Schematic diagram of peak points classification based on prior information of transmitted signal.

The determination of the range of the fuzzy region is indeed the determination of the maximal Doppler frequency f_{d-max} . It is related to the maximal relative velocity v_{max} between the object to be detected and the radar station, complying with the following equation:

$$f_{d-max} \approx \frac{|v_{max}|}{c} f_0, \quad (6)$$

where c is the speed of light, and f_0 is the center frequency of transmitted signal. Usually, the velocity v_{max} is set as large as possible to ensure the validity of the classification shown in Fig. 4.

In the picking of the peak points in the 'energy lines', there is a magnitude threshold labeled by $M_{T(dB)}$ here (in 'dB' form). For one column of the data in the valid region of $|\chi(\tau, f)|$, only the maximal point larger than $M_{T(dB)}$ is thought to be a valid peak point (in an 'energy line') and is picked. The threshold is determined by the following equation:

$$M_{T(dB)} = |\chi(\tau, f)|_{\max(dB)} - C_{T(dB)}, \quad (7)$$

where $|\chi(\tau, f)|_{\max(dB)}$ is the maximum of $|\chi(\tau, f)|$ in 'dB' form, and $C_{T(dB)}$ is a const value in 'dB' form indicating the boundary of the main energy region of the components. The value $C_{T(dB)}$ is set as 6dB here. In some extreme case where the echo signal is extreme weak, one can consider to set a smaller $C_{T(dB)}$ (such as the half-power boundary 3dB) to obtain a more stable results.

After picking the points and classifying them, one can evaluate the undetermined parameters of the two

'energy lines'. Actually, by using the 'part b' prior information of the transmitted signal listed before, we find that there are only two undetermined parameters b_1 and b_2 , which comply with the following equations:

$$b_1 = f_{p1} + \frac{B}{T} \tau_{p1}, \quad (8a)$$

$$b_2 = f_{p2} - \frac{B}{T} \tau_{p2}, \quad (8b)$$

where (τ_{p1}, f_{p1}) and (τ_{p2}, f_{p2}) are the time-frequency coordinate of a picked point in 'line1' and that in 'line2', respectively.

The optimal b_1 and b_2 are labeled as $b_{1(opt)}$ and $b_{2(opt)}$, respectively. They are the solution of the following optimization problem:

$$b_{1(opt)} = \arg \min_{b_1} \sum_{n=1}^{N_1} \left(b_1 - \left(f_{p1(n)} + \frac{B}{T} \tau_{p1(n)} \right) \right)^2, \quad (9a)$$

$$b_{2(opt)} = \arg \min_{b_2} \sum_{n=1}^{N_2} \left(b_2 - \left(f_{p2(n)} - \frac{B}{T} \tau_{p2(n)} \right) \right)^2, \quad (9b)$$

where N_1 and N_2 are the number of picked points in 'line1' and that in 'line2', respectively, and $(\tau_{p1(n)}, f_{p1(n)})$ and $(\tau_{p2(n)}, f_{p2(n)})$ are the coordinate of the n -th picked point in 'line1' and that in 'line2', respectively.

The optimization problem (9a) and (9b) just can be solved by the least square method which can generate the optimal results in the sense of minimizing the energy of error. Whereas the undetermined parameter here is only one for one problem (9a) or (9b), so the solution form is simple, as shown below:

$$b_{1(opt)} = \frac{1}{N_1} \sum_{n=1}^{N_1} \left(f_{p1(n)} + \frac{B}{T} \tau_{p1(n)} \right), \quad (10a)$$

$$b_{2(opt)} = \frac{1}{N_2} \sum_{n=1}^{N_2} \left(f_{p2(n)} - \frac{B}{T} \tau_{p2(n)} \right). \quad (10b)$$

Replacing b_1 and b_2 in (8a) and (8b) by $b_{1(opt)}$ and $b_{2(opt)}$ respectively, then combining (8a) and (8b) to be simultaneous equations and solving the variables f and τ , we obtain the evaluation of the crossing point of the two components. By simplification of the result, the time delay τ_E and Doppler frequency f_{d-E} of the crossing point can be expressed as follows:

$$\begin{cases} \tau_E = \frac{(b_{1(opt)} - b_{2(opt)})T}{2B}, \\ f_{d-E} = \frac{b_{1(opt)} + b_{2(opt)}}{2}. \end{cases} \quad (11)$$

Obviously, τ_E and f_{d-E} correspond to the estimated time delay and estimated Doppler frequency of the object to be detected, respectively. The error of τ_E and that of f_{d-E} can then be defined as:

$$\begin{cases} \Delta\tau_E = \tau_E - \tau_{True} \\ \Delta f_{d-E} = f_{d-E} - f_{d-True}, \end{cases} \quad (12)$$

where τ_{True} and f_{d-True} denote the true time delay and true Doppler frequency of the object, respectively.

IV. SIMULATIONS

In this section, we will illuminate the validity of the proposed method. Also we will give a comparison of the method to the common FRFT-based method to show its superiority. The software for simulation is MATLAB R2014, and the computer hardware setting is as follows: CPU: Intel Core i5 3.3GHz, Memory: 8GB, OS: Windows7-64bit.

To show the validity of the proposed method, the noise is considered in the simulation. The signal-noise-ratio (SNR) is employed to measure the noise level, which is defined as follows:

$$SNR = 10 \log_{10}(P_S / P_n), \quad (13)$$

where the unit of SNR here is dB, and P_S and P_n are the power of signal (echo signal without noise) and that of noise, respectively. As for each test SNR, we make statistical measures with 100 times (generating 100 noise samples). For each noise sample, we test four block sizes of the time-frequency matrix obtained by ambiguity function. Some common parameters settings are given as below. The center frequency of transmitted signal is $f_0 = 2.7\text{GHz}$, the model of transmitted signal is adopted as a 2-component LFM signal as shown in Sec. III. The plasma effect is selected to be the same case described in the purple dashed line in Fig. 1, which is a severe case for the selected transmitted radar signal. The default true time delay and Doppler frequency of an object is set as 3.5us and 342KHz, respectively.

A. Validation of the proposed method

A fixed transmitted signal is simulated with pulse

width 50us and bandwidth 100MHz. One can find that the ambiguity resolutions of this transmitted signal in time delay and Doppler frequency are 10ns (1/100MHz) and 20KHz (1/50us), respectively. In the calculation of ambiguity function, the discrete size (or block size) of the generated function needs to be considered. Clearly, larger size can provide finer time-frequency structure which is helpful for estimation, but it will be more time-consuming. In contrast, smaller size case provides coarser time-frequency structure but is more efficient in calculation. As a simplification, the generated figures of ambiguity function are considered to be square (the same number of rows and columns). We select four different block sizes (number of rows or columns) for test: [500, 250, 125, 63], which are in a reasonable range for real-time radar detection. Figure 5 shows the estimation errors for the time delay and Doppler frequency by the proposed method for the four block sizes at SNRs of -20dB, -10dB, and 0dB, respectively. For each selected SNR and block size, there are 100 results generated corresponding to 100 noise samples and drawn in Fig. 5.

As shown in Fig. 5, the estimated time delay and Doppler frequency tend to concentrate with the increase of SNR. As for the block size, its influence on the concentration of estimation results is trivial, but it will affect the deviation of the results. Usually, the smaller the block size, the larger the deviation of estimated results.

Whereas the most important fact observed from Fig. 5 is that the proposed method can work in an acceptable way even at an extreme SNR of -20dB (see Fig. 5 (a)). In this extreme SNR case, the estimated results are still not over the ambiguity resolution (10ns in time delay and 20KHz in Doppler frequency) and have not generate 'bad point', which shows the high estimated accuracy and stability of the proposed method.

To show the deviation and error of the estimated time delay and Doppler frequency from a quantitative view, we calculate the average deviation and the std (standard deviation) of the estimated results. The tested SNRs are extended to five cases for sufficient test: -20dB, -15dB, -10dB, -5dB, and 0dB. Let $|\overline{\Delta\tau_E}|$ be the absolute average error of time delay and $|\overline{\Delta f_{d-E}}|$ be the absolute average error of Doppler frequency. Let $\delta_{\Delta\tau_E}$ be the std of time delay error and $\delta_{\Delta f_{d-E}}$ be the std of Doppler frequency error. Fig. 6 shows the statistic results of the average deviation and std.

As presented in Fig. 6, the average deviation of time delay and that of Doppler frequency are both insensitive to SNR. Whereas they can be affected by the block size distinctively. In general, larger block size is more possible to generate smaller estimated deviation, which conforms to the results in Fig. 5. As for the std of estimated error, the influence of SNR predominates.

With the increase of SNR, the stds of estimated errors both for time delay and Doppler frequency decrease.

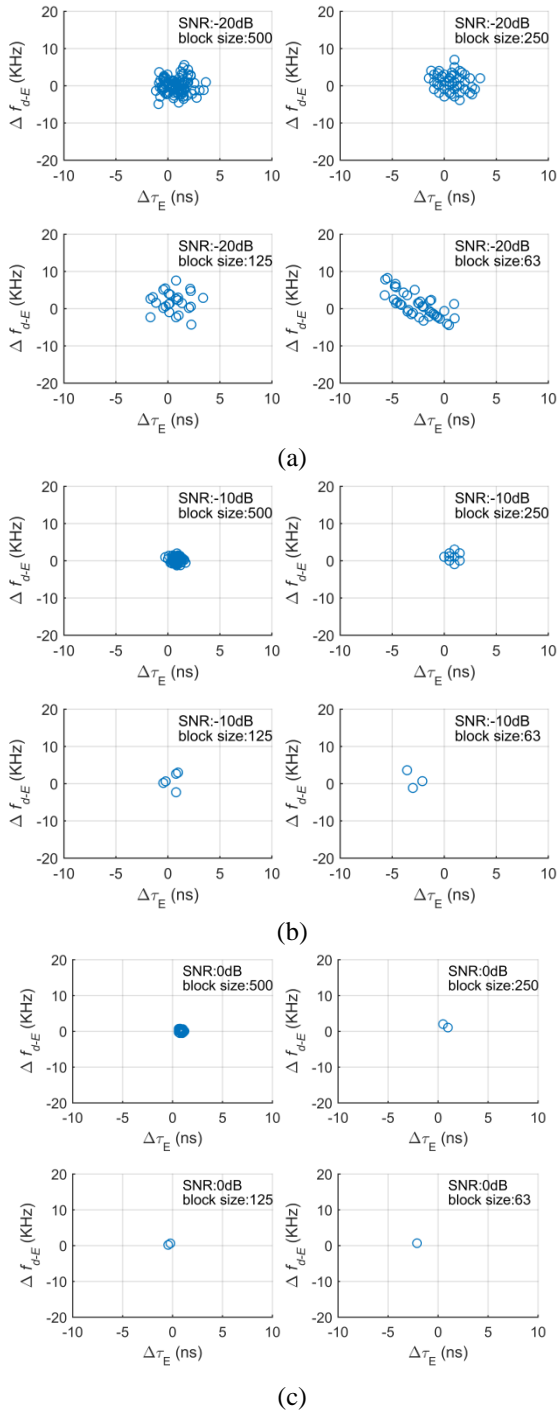


Fig. 5. The estimation errors for time delay $\Delta\tau_E$ and Doppler frequency Δf_{d-E} for 4 block sizes of time frequency matrix at different SNRs. (a) SNR=-20dB, (b) SNR=-10dB, and (c) SNR=0dB.

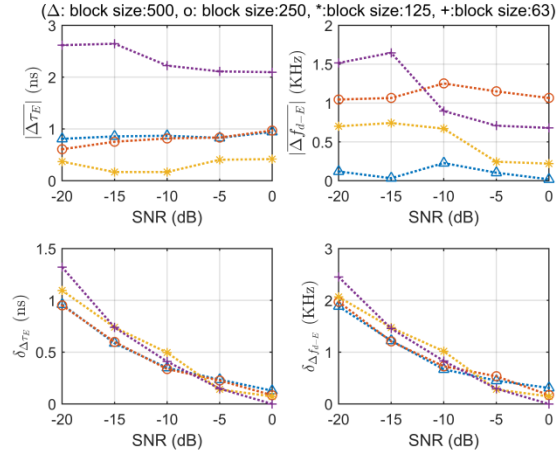


Fig. 6. Average deviation and std of the estimated time delay and Doppler frequency by the proposed method. Top left: absolute average error of time delay $|\Delta\tau_E|$ vs SNR; top right: absolute average error of Doppler frequency $|\Delta f_{d-E}|$ vs SNR; bottom left: std of time delay error $\delta_{\Delta\tau_E}$ vs SNR; bottom right: std of Doppler frequency error $\delta_{\Delta f_{d-E}}$ vs SNR.

One can also find that the maximal deviation of estimated time delay is not larger than 3ns and that of the Doppler frequency is not larger than 1.5KHz. Both of them are lower than the ambiguity resolution (10ns for time delay and 20KHz for Doppler frequency) significantly. As for the stds of estimated errors, they are also much lower than the ambiguity resolution even for the extreme SNR of -20dB.

For the time consumption, the proposed method also has superiority. Actually, the most time-consuming part of the method lies in the calculation of ambiguity function. In the simulation of Fig. 5, at any a fix SNR and a fixed noise sample, the algorithm consumes near the same time of about 0.5s for each block case without considering the calculation of ambiguity function. For the calculation of ambiguity function, it takes about 10.4s, 5.6s, 2.8s, and 1.6s for the block sizes 500, 250, 125, and 63, respectively. Certainly, in the calculation of ambiguity function, the fast algorithm is employed. However, one should note that the simulation in this paper does not utilize the parallel computing. Whereas in the realistic application, the parallel computing is highly suggested, which can further significantly reduce the consumed time.

B. Comparison of the proposed method to FRFT-based method

To evaluate the proposed method fairly, we employ the common FRFT-based method to estimate the time

delay and Doppler frequency. For fair comparison, the related parameters are set same with that by the proposed method shown above. The block sizes of the angle-shift region in FRFT are set as [500, 250, 125, 63], the same with that in Sec. VI-A. Figure 7 shows the estimated results for SNR=-20dB.

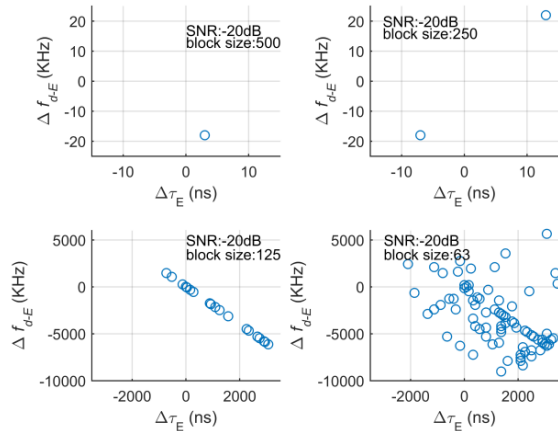


Fig. 7. The estimation errors for time delay $\Delta\tau_E$ and Doppler frequency Δf_{d-E} by FRFT for four block sizes at SNR=-20dB.

As for the block cases 500 and 250 as shown in Fig. 7, the maximal divergences of estimated results have reached about 20KHz for Doppler frequency and 10ns for time delay even though the results have better concentration. As for the cases with block sizes 125 and 63, however, the estimated results are flawed. Comparing these results with that by the proposed method as shown in Fig. 5 (a), one can find the resulting deviation by the proposed method is smaller (not larger than half of that by FRFT). Furthermore, as for the block sizes 125 and 63, the proposed method also generates acceptable result with smaller deviation.

The detailed estimated results for other SNRs are not shown here for saving space. Instead, we calculate the average deviation and the std of the estimated results for all the five candidate SNRs (including -20dB, -15dB, -10dB, -5dB, and 0dB) and present them in Fig. 8. Considering the huge estimation errors for blocks 125 and 63 at lower SNRs, we separate these blocks into two groups and plot the results in two sub-figures, as shown in Figs. 8 (a) and (b).

As shown in Fig. 8 (a), the average deviation and the std for the block sizes 125 and 63 do not reach a 'normal level' until the SNR gets to a larger level (≥ -10 dB here). Yet the average deviation in the 'normal level' is still much larger than that by the proposed method in Fig. 6, even though the std reaches zero. Take a look at the case of SNR=0: for $|\Delta f_{d-E}|$, the deviation reaches 141.9KHz for block size 63 and 19.4KHz for block size 125; for

$|\Delta\tau_E|$, it reaches 7.4ns for the two block sizes. For block sizes 500 and 250 in Fig. 8 (b), the estimated results appear to be stable ($\delta_{\Delta\tau_E} = \delta_{\Delta f_{d-E}} = 0$) for SNR ≥ -15 dB. Whereas, the average deviations are nearly not affected by the SNR and are in a higher level than that by the proposed method in Fig. 6. For SNR ≥ -15 dB, $|\Delta f_{d-E}|$ reaches 18KHz for both the block sizes 500 and 250, and $|\Delta\tau_E|$ reaches 7ns for block size 250 and 3ns for block size 500.

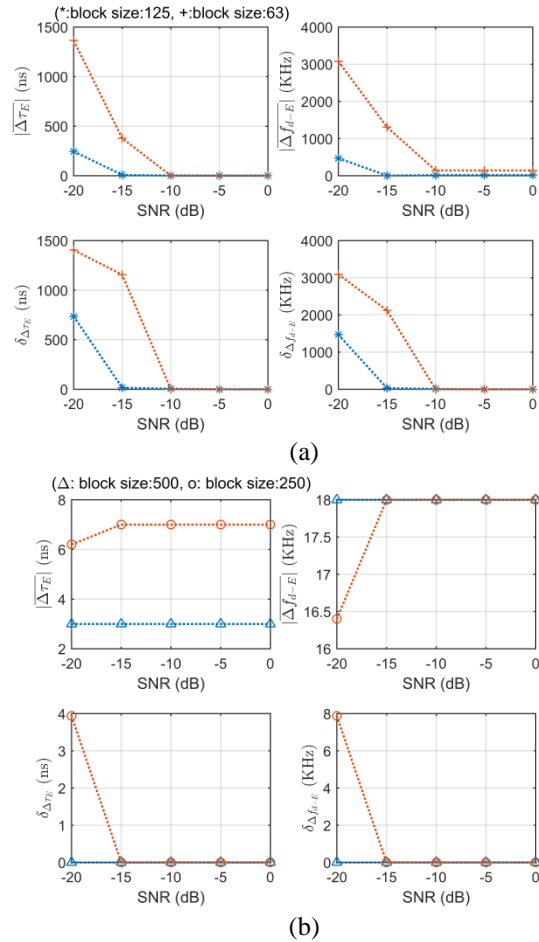


Fig. 8. Average deviation ($|\Delta\tau_E|$ and $|\Delta f_{d-E}|$) and std ($\delta_{\Delta\tau_E}$ and $\delta_{\Delta f_{d-E}}$) of the estimated time delay and Doppler frequency by FRFT. (a) Block sizes: 125 and 63. (b) Block sizes: 500 and 250.

The larger deviations of the estimated results by FRFT are mainly due to that the estimation precision mainly relies on the setup of increment (or the block size mentioned here), as indicated in the Introduction Section. Whereas, given the same block size, the proposed method makes full use of the block information (exactly, the 'energy line' information) and the prior information,

with the estimation results solved by an optimal scheme on those information. This results in a much higher improvement in estimation, as shown in Fig. 5 and Fig. 6.

For the time consumption, at any a fix SNR and a fixed noise sample, it is about 1210s for calculating all the four block cases in all, including 894s, 244s, 57s, and 15s for the block sizes 500, 250, 125, and 63, respectively. It is very time-consuming compared with the proposed method. The applicable fast algorithm of FRFT in the scenarios of this paper is in the consideration of our further work.

In all, the simulation results above show the validity of the proposed method in precision and efficiency. In addition, the results also illustrate the stability of the proposed method, in which acceptable estimation results are generated without ‘bad point’ even for SNR=-20dB. The comparison to FRFT-based method further shows the superior of the proposed method in solving the radar detection problem of plasma-covered objects.

V. CONCLUSION

In this paper, we proposed a precise and efficient radar detection method based on crossed 2-component LFM signal to deal with the detection problem of plasma-covered objects. By designing the transmitted signal to be a crossed 2-component LFM signal and detecting the object information from the ambiguity function of echo signal, the accuracy and efficiency are achieved. The simulation results illustrate the validity of the proposed method in accuracy, efficiency, and stability in estimating the object information (position and velocity). In our further work, some more extreme cases for plasma influence will be studied and also the detection of multiple objects will be considered.

ACKNOWLEDGMENT

This work was supported by the National Science Foundation of China under Grants 61701380, the Science and Technology on Space Physics Laboratory Funds, and the China Postdoctoral Science Foundation (No. 2016M592758).

REFERENCES

- [1] J.-T. Li and L.-X. Guo, “Research on electromagnetic scattering characteristics of reentry vehicles and blackout forecast model,” *J. Electromagnet. Wave*, vol. 26, no. 13, pp. 1767-1778, 2012.
- [2] H. Torres-Silva, N. Reggiani, and P. H. Sakanaka, “Electromagnetic properties of a chiral-plasma medium,” *ACES Journal*, vol. 12, no. 1, pp. 14-18, 1997.
- [3] W. Liu, J. Zhu, C. Cui, and X. Wang, “The influence of plasma induced by α -particles on the radar echoes,” *IEEE Trans. Plasma Sci.*, vol. 43, no. 1, pp. 405-413, 2015.
- [4] S.-H. Liu and L.-X. Guo, “Analyzing the electromagnetic scattering characteristics for 3-D inhomogeneous plasma sheath based on PO method,” *IEEE Trans. Plasma Sci.*, vol. 44, no. 11, pp. 2838-2843, Nov. 2016.
- [5] M.-Y. Wang, H.-L. Li, Y.-L. Dong, G.-P. Li, B.-J. Jiang, Q. Zhao, and J. Xu, “Propagation matrix method study on THz waves propagation in a dusty plasma sheath,” *IEEE Trans. Antenn. Propag.*, vol. 64, no. 1, pp. 286-290, Jan. 2016.
- [6] X. Chen, K. Li, Y. Liu, Y. Zhou, X. Li, and Y. Liu, “Study of the influence of time-varying plasma sheath on radar echo signal,” *IEEE Trans. Plasma Sci.*, vol. 45, no. 12, pp. 3166-3176, Dec. 2017.
- [7] S. V. Bobashev and Y. P. Golovachov, “Deceleration of supersonic plasma flow by an applied magnetic field,” *J. Propul. Power*, vol. 19, no. 4, pp. 538-546, July 2003.
- [8] M. Kim, M. Keidar, and I. D. Boyd, “Analysis of an electromagnetic mitigation scheme for reentry telemetry through plasma,” *J. Spacecraft Rockets*, vol. 45, no. 6, pp. 1224-1229, Nov. 2008.
- [9] I. F. Belov, V. Y. Borovoy, V. A. Gorelov, A. Y. Kireev, A. S. Korolev, and E. A. Stepanov, “Investigation of remote antenna assembly for radio communication with reentry vehicle,” *J. Spacecraft Rockets*, vol. 38, no. 2, pp. 249-256, Mar. 2001.
- [10] Y. Zhou, X. Chen, K. Li, Y. Liu, and Y. Liu, “The application of multi-component LFM signals to radar detection of plasma-covered reentry object,” in *2017 International Applied Computational Electromagnetics Society Symposium (ACES 2017)*, Suzhou, China, p. 1937, Aug. 2017.
- [11] J. Su, H.-H. Tao, X. Rao, and J. Xie, “Coherently integrated cubic phase function for multiple LFM signals analysis,” *Electron. Lett.*, vol. 51, no. 5, pp. 411-413, 2015.
- [12] P. Wang, J.-Y. Yang, and Y.-M. Du, “A fast algorithm for parameter estimation of multi-component LFM signal at low SNR,” *IEEE Int. Conf. Communications, Circuits and Systems Proceedings*, Hong Kong, China, vol. 2, pp. 765-768, 2005.
- [13] H.-T. Qu, R.-H. Wang, W. Qu, and P. Zhao, “Research on DOA estimation of multi-component LFM signals based on the FRFT,” *Wireless Sensor Network*, vol. 1, no. 3, pp. 171-181, 2009.
- [14] F. Liu, H.-F. Xu, R. Tao, and Y. Wang, “Research on resolution between multi-component LFM signals in the fractional Fourier domain,” *Science China: Information Sciences*, vol. 55, no. 6, pp. 1301-1312, June 2012.
- [15] Q. Guo, Y.-J. Li, C.-H. Wang, and H.-Y. Cao, “Novel detection method for multi-component LFM signals,” *Int. Conf. Pervasive Computing Signal Processing and Applications (PCSPA)*,

Harbin, China, pp. 759-762, Sept. 2010.

- [16] Y.-X. Li and X.-C. Xiao, "Recursive filtering radon-ambiguity transform algorithm for detecting multi-LFM signals," *Chinese J. Electron.*, vol. 20, no. 3, pp. 161-166, May 2003.
- [17] P. W. Huber, N. D. Akey, W. F. Crosswell, and C. T. Swift, "The entry plasma sheath and its effects on space vehicle electromagnetic systems," *NASA, Washington, DC, USA, Tech. Note SP-252*, p. 1-630, 1971.



Xuyang Chen was born in Hebei, China, in 1980. He received the B.S., M.S., and Ph.D. degrees in Electronic Engineering from Xidian University, Xi'an, China, in 2005, 2008, and 2011, respectively. He joined the CAST-Xi'an Institute of Space Radio Technology, Xi'an, as an Engineer in 2011, where he is involved in radar detection and space navigation. He is currently a Teacher with the School of Aerospace Science and Technology, Xidian University. His current research interests include the radar detection of reentry vehicles covered by plasma sheath.



Fangfang Shen received the B.S., M.S. and Ph.D. degrees in Telecommunications Engineering from Xidian University, Xi'an, China, in 2006, 2009, and 2015, respectively. She is currently a Teacher with the School of Aerospace Science and Technology, Xidian University. Her research interests include high-resolution radar imaging and DOA estimation.



Yanming Liu was born in Shaanxi, China, in 1966. He received the B.S., M.S., and Ph.D. degrees from Xidian University, Xi'an, China, in 1989, 1993, and 2003, respectively. He is currently a Full Professor with the School of Aerospace Science and Technology, Xidian University. His current research interests include telecommunication network technology and wireless communication.



Xiaoping Li was born in Shanxi, China, in 1961. She received the B.S., M.S., and Ph.D. degrees from Xidian University, Xi'an, China, in 1982, 1988, and 2004, respectively. She is currently a Full Professor with the School of Aerospace Science and Technology, Xidian University. Her current research interests include telemetry, tracking and command technology.



Wei Ai was born in Shanxi, China, in 1977. He received the B.S. degree from North University of China in 2000, and M.S. degrees from China Academy of Launch Vehicle Technology in 2011. He is currently a senior Engineer with China Academy of Launch Vehicle Technology. His current research interests include communication technique and system integration design.